Structures of Apomyoglobin's Various Acid-Destabilized Forms†

Rudolf Gilmanshin,‡,§ Miriam Gulotta,‡ R. Brian Dyer,|| and Robert H. Callender*,‡

Department of Biochemistry, Albert Einstein College of Medicine, Bronx, New York 10461, and Bioscience Division, Mail Stop J586, Los Alamos National Laboratory, Los Alamos, New Mexico 87545

Received September 25, 2000; Revised Manuscript Received December 5, 2000

ABSTRACT: The structures and the cold and hot melting thermodynamics of the acid- and salt-destabilized states of horse heart apomyoglobin (apoMb), including the E (extended) and various I forms, are studied using probes of tertiary structure (tryptophan fluorescence and FTIR spectroscopy) and secondary structure (far-UV CD and FTIR spectroscopy). These forms likely resemble early structures in the folding of the largely helical protein. Both the I and E forms retain the AGH core whereby the two ends of the protein are tied together with sufficient numbers of tertiary contacts, involving a number of hydrophobic residues, to show cooperative melting. The melting thermodynamics of E and I are distinctly different. E contains no other tertiary structure and probably little other secondary structure apart from the core. The more destabilized E form appears to contain "random" buried runs of polypeptide backbone which convert to α-helix in the I form(s). Most interestingly, E consists not of a single structure but is composed of a heterogeneous mixture of conformations, all showing corelike cooperative melting characteristics, and consisting presumably of varying contacts between the A portion of apomyoglobin and the G−H hairpin. These results bear on the energy landscape and structural features of the early part of apomyoglobin's folding pathway.

The equilibrium, acid-destabilized forms of apomyoglobin are of substantial interest in the study of the protein folding problem. This is in part because of the attractive features of apoMb[1] itself as a model for folding, including a relatively simple topology and secondary structure content (mostly helical) and a lack of features that complicate folding such as prosthetic groups, disulfide linkages, or prolines. Figure 1 shows a ribbon diagram of the crystal structure of myoglobin (PDB entry 1AZI), which is close in structure to the native conformation of the apoprotein (*1*, *2*). The acid-destabilized forms of the protein are even simpler in some respects, because they are partially unfolded yet contain a residual compact core with stable secondary and tertiary structures. At least three low-pH forms of apoMb (I, I′, and E; vide infra) can be stabilized and significantly populated by varying the pH and ionic strength. Pulsed deuterium labeling NMR and mass spectrometry studies have demonstrated that at least one of these forms (I) is also an obligatory kinetic folding intermediate (*3*−*5*). The structures and dynamics of these partially unfolded forms therefore offer intriguing insight into the mechanism of folding. The progressively destabilized forms of the protein may represent earlier and earlier intermediates, if the most stable parts of the protein form first. Even if these forms do not represent productive folding intermediates, however, they are still intriguing because they begin to probe the upper reaches of the folding energy landscape, thus revealing properties of that landscape not normally seen in experiments that only probe the starting and final states.

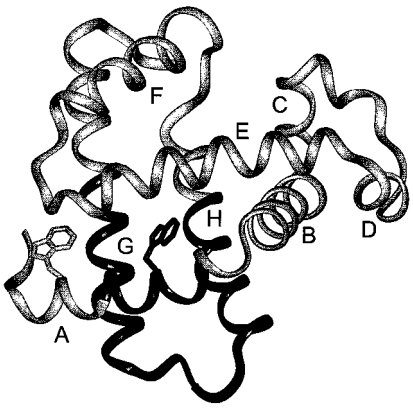

FIGURE 1: Ribbon diagram of the structure of horse heart myoglobin (1AZI) with the heme not shown. The locations of the eight helices (labeled A−H) are shown. Myoglobin's two tryptophan residues, Trp7 and Trp14, are shown. The AGH core which exists in the E conformation has been darkened.

Three equilibrium forms of apoMb [U (unfolded; pH ≤2.0, low ionic strength), I (intermediate; pH 4.2), and N (native; pH ≥5.3)] have been known for some time (*6*−*9*). More recently, we discovered a particularly destabilized form of the protein (formed at pH 3 and low ionic strength) called E (for extended) because it appears to be substantially unfolded and extended (*10*). In addition, it is possible to produce a

† This work was supported by the National Science Foundation (Grant MCB-9727439 to R.H.C.) and the Institute of General Medicine, National Institutes of Health Grants GM53640 (R.B.D.) and GM35183 (R.H.C.).

* To whom correspondence should be addressed. Phone: (718) 430-3024. Fax: (718) 430-8565. E-mail: call@aecom.yu.edu.

‡ Albert Einstein College of Medicine.

§ Current address: U.S. Genomics, Inc., 8 Saint Mary's St., Suite 922, Boston, MA 02215.

|| Los Alamos National Laboratory.

[1] Abbreviation: apoMb, myoglobin with the prosthetic heme group extracted.

10.1021/bi002255v CCC: $20.00
Published on Web 04/04/2001

variation of the I form, I′, at lower pH values and specific ionic strengths that appears to be thermodynamically and structurally distinct from I (*10*) and which was called I_a in ref *9*. The eight helical runs of apoMb (see Figure 1) are mostly intact in the native (most stable) form (*4*), which is estimated to contain about 55% helix (see refs *10* and *11* and below). The structure of the holoprotein shown in Figure 1 is about 80% helical. The structure becomes increasingly disordered in the pH-destabilized forms yet retains a significant helical content. Apart from a small number of isolated helical turns, apoMb is essentially unfolded at pH 2 in the absence of salt.

The E and I forms of apoMb contain a distinctive structure, the AGH core, which is composed of some 20−40 residues at the intersection of the A helix with the G and H helices and the G−H hairpin turn and includes part of the B helix, at least in I (*4*, *8*, *12*−*14*). The central part of the core has been shaded in black in Figure 1. Hence, the two ends of apoMb are tied together when the AGH core is formed. This core is compact and melts cooperatively. NMR folding studies of the formation of native apoMb, monitoring hydrogen−deuteron exchange kinetics, show that the amide protons in the AGH core are highly protected in the ∼5 ms burst phase of these experiments (*3*). Using laser-induced temperature-jump techniques, we have shown that the AGH core of E is formed within 96 μs at physiological temperatures, which is close to the diffusion limit for the formation of a loop tied at two ends from a disordered polypeptide the size of unfolded apoMb (*15*). Thus, the fast formation of the AGH core appears to be a critical early step in the folding of apoMb (*3*, *4*, *7*, *9*, *14*, *15*).

The purpose of this work is to investigate the detailed structures and the thermodynamics of the cold- and heat-denaturation transitions for the various acid-denatured forms of apoMb, using Trp fluorescence, infrared absorbance (IR), and circular dichroism (CD) spectroscopies. There is already a wealth of structural information for the I form, including a recent NMR structure at 50 °C with a specific counterion (acetate) for sperm whale apoMb (*4*). The latter study also characterized the unfolded state (pH 2.3, no added salt). The structures of apoMb for other conditions (i.e., close to that of E), however, have been unclear. In addition, most structural studies of acid-destabilized apomyoglobin have been performed on sperm whale apomyoglobin. Our fast folding kinetics studies (*15*−*18*) have been on the horse heart protein in D_2O (the latter required for IR kinetics). Although it is unlikely that apoMb from horse versus sperm whale or the use of H_2O versus D_2O would introduce any dramatic changes in the structures of the various acid-denatured forms, the structural and thermodynamic studies presented here were performed under exactly the same conditions that were used in the fast kinetics studies. The following paper investigates the temperature-jump relaxation dynamics of the E state in greater detail (*19*).

Our approach in the current work is to use a suite of spectroscopic techniques that provide complementary information about the acid-destabilized structures. We have previously studied the melting behavior of apoMb under various destabilizing conditions using Trp fluorescence to monitor the melting of the AGH core (*10*). There are two Trp residues in the horse heart protein, and both are located in the A helix (Trp7 and Trp14). The indole rings of these Trp residues are partly buried in the AGH core of the native protein, as can be seen in Figure 1. As the protein unfolds, the Trps become more and more solvent exposed, dramatically changing their fluorescence properties, until they are fully exposed in the U form. Thus, Trp fluorescence has been used as a monitor of the presence of the AGH core. In this work, we have used Trp fluorescence to study the effects of both temperature and systematic titration with various salts. Cooperative (sigmoidal) transitions are induced by both temperature and changes in ionic strength, characteristic of a compact AGH core containing specific tertiary interactions (ref *10* and below). We have also performed parallel structural measurements monitoring the amide I′ absorption band of the protein (the prime indicates samples exchanged in D_2O, which contain deuterated amide linkages) and far-UV CD. Both the protein IR amide I′ band and its far-UV CD spectrum are sensitive probes of protein secondary structure and so give information that is complementary to the Trp fluorescence measurements. Finally, the amide I′ band also reports on the compactness of the core.

MATERIALS AND METHODS

Materials. The preparation and purification of horse apoMb samples have been described in detail previously (*10*). A stock apomyoglobin solution was prepared by first dissolving the lyophilized apomyoglobin in the appropriate solvent, adjusting the pH* accordingly using a minimal amount of DCl. The pH* is the uncorrected (for D_2O) pH-meter reading at room temperature. Lyophilized protein always includes residual salt and water. As the apoMb structure at low pH is extremely sensitive to the actual salt concentration, gel filtration on a Sephadex G25 column was performed to remove any excess salt as well as separate out any aggregates from the protein solution. For FTIR spectroscopy, the buffer fraction immediately preceding the protein peak was collected and used as a reference to ensure the precise balance of residual HOD. The collected protein solution was isolated as it left the column. Aliquots of the eluted fractions were used to determine protein concentration [$\epsilon_{280} = 1.43 \times 10^4$ M^{-1} cm^{-1} or $E_{280}^{1\%} = 8.4$ cm^{-1} (*20*)].

The apoMb-E solution contained 20 mM NaCl at pH* 3.0. The apoMb-I′ is at pH* 3 and high salt (>100 mM), while the apoMb-I solution included 10 mM sodium acetate at pH* 4.2 with no other salts. The NaCl titration measurements were performed by mixing two protein solutions with the same concentration and pH*. One of them had a fixed concentration of NaCl; the other one had no extra salt. The NaCl concentrations of the mixed solutions were calculated from the measured weights of the aliquots and their known densities. The reversibility of the temperature denaturation was checked by scanning upward to a specific high temperature and then cooling. Excellent reversibility was found below 55 °C under all conditions. At higher temperatures, reversibility depended upon protein concentration, conditions, and the time interval of exposure to high temperatures. No data are shown here unless reversibility was within 10%, and some of the data plots show the results of this control.

Fluorescence Measurements. Fluorescence spectra were recorded on a FluoroMax-2 spectrofluorimeter (Instruments S. A., Inc.) with correction for a spectral dependence of registration response. The excitation wavelength was 290 nm.

Similar results were obtained using 275 nm excitation. A 3 nm band-pass was used for both excitation and emission. Samples with concentrations of 0.05 mg/mL in a 1 cm square fused-silica cuvette were used. The data were collected and processed with the DataMax software (Instruments S. A., Inc.). See ref *10* for other details.

Infrared Spectroscopy. Static infrared spectra were obtained using a Bruker model IFS 66 FTIR spectrometer as described previously (*21*). Sample concentrations of 4−8 mg/mL were used for the IR measurements. No aggregation was observed (marker amide I bands indicative of aggregation are readily observed) in equilibrium measurements at concentrations of <5 mg/mL if the time of exposure to high temperatures (>60 °C) did not exceed 2 h. The second derivatives were smoothed with a fourth-order, 19-point Savitzky−Golay algorithm (which corresponds to ~20 cm^{-1} band-pass filter). Teflon spacers of 50 μm were used for the equilibrium measurements.

CD Spectroscopy. CD spectra were taken on a Jasco J-720 spectrometer equipped with a temperature-controlled cuvette holder. The spectrometer was calibrated using D-camphorsulfonic acid. Rectangular 1 mm path length quartz cuvettes were used for the measurements. Each spectrum is an average of two scans taken between 300 and 190 nm at either 50 or 100 nm/min. The sensitivity setting was 20 mdeg, and the response time was 4 s. The slit width was set at 1.0 mm which gave a 0.5 nm resolution. The data were analyzed by subtracting any background CD spectrum and converting the spectra from millidegrees to molar ellipticity ([Θ]) in degrees per square centimeter per decimole. A stock protein solution with a known concentration was added to a solution of the same solvent to make a final solution with a concentration between 0.01 and 0.02 mg/mL. The final solution was then scanned in the UV spectrometer to ensure that the absorbance below 200 nm was not >1. Analysis of secondary structure content was carried out using software obtained from the web site of the University of Medicine and Dentistry of New Jersey Circular Dichroism Facility in Piscataway, NJ. The analysis package was CONTIN version 2DP (*22*).

RESULTS

The structure of apoMb is very sensitive to the pH and ionic strength of the solution. The A helix of the AGH core contains the only two tryptophan residues of the protein (Trp7 and Trp14), and the λ_{max} of their intrinsic fluorescence spectra provides a means of monitoring core formation because of the indole ring's sensitivity to its surroundings (*10*). Figure 2 presents fluorescence titration curves of apoMb against NaCl or NaI at pH* 3.0 and 2.0. The protein has an uncompensated positive charge at these low pH values that produces a strong electrostatic repulsion and acts as the main driving force of unfolding. The total charge uptake for the N → I transition has been estimated from NMR pH titrations to be ~2, with the biggest contribution from H24 (*23*). The uncompensated charge is neutralized by the addition of anions, provided by either a decrease in the pH or addition of anions with salts (*24*), causing the protein to partially refold. At the lowest measured anion ion concentration at pH* 2, the λ_{max} of the apoMb tryptophan fluorescence is nearly the same as that of free L-Trp in solution, indicating that the Trp side chains are nearly completely exposed to solvent. Addition of NaCl or NaI results in a sharp structural transition expressed as a blue shift of the fluorescence spectrum. At pH* 3, a single transition is observed for the iodide titration, which is nearly over at 30 mM I^-. Its λ_{max} at high salt lies at 328 nm, which is strongly blue shifted relative to that of the chloride. On the other hand, two apparent transitions are observed for the chloride titration at pH* 3. The first transition is nearly complete at 20 mM NaCl, the conditions we have identified to produce the E form in our previous studies (*10*, *15*). A second transition is evident with further increases in salt concentration, although with a less steep dependence. At the high concentration limit (>160 mM; full data range not shown), where apoMb adopts an I form (*11*, *24*), the position of the emission spectrum is nearly the same as that of the native protein (*10*, *24*). We have called the pH* 3, high-salt form I′ to distinguish it from I, generally taken to refer to pH* 4.2 at any salt concentration. It is formed under conditions similar to those of the I_a form found by Baldwin and co-workers (*9*). At pH* 2.0, the screening of Trp side chains begins at higher ionic strength than at pH* 3.0, proceeds as a single transition, and ends at 100 mM NaCl, i.e., with formation of the I′ form. For comparison, the λ_{max} of I, formed at pH* 4.2 with 10 mM sodium acetate, is plotted in Figure 2. It lies at 332 nm, showing that the tryptophan side chains are highly screened from solvent, and this value is essentially the same as that found in I′. Similar studies using other cation salts (CsCl and KI) yielded results identical to those for NaCl and NaI, respectively, indicating that the cation of the salt is not important, as expected (*25*).

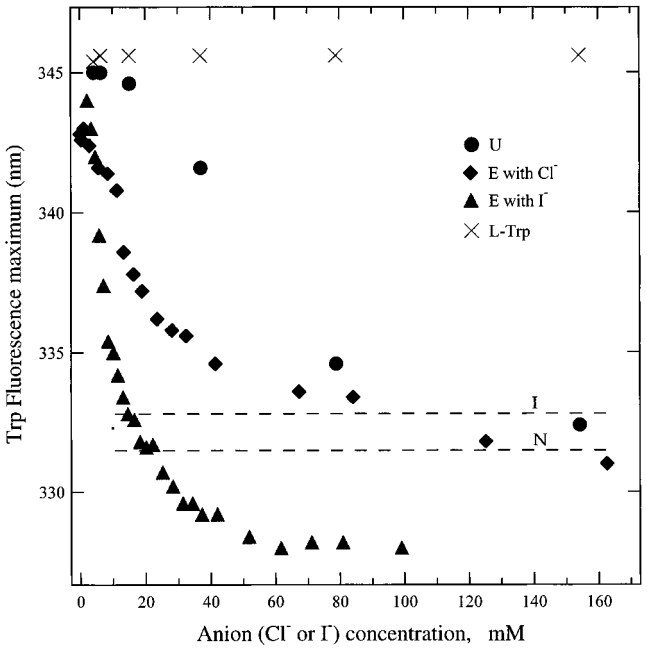

FIGURE 2: Maximum wavelength (λ_{max}) of the intrinsic fluorescence spectrum of horse heart apoMb as a function of chloride or iodide anion concentration. The λ_{max} values of apoMb fluorescence at pH* 2.0 titrated with Cl^- (●), pH* 3.0 titrated with Cl^- (◆), pH* 3.0 titrated with I^- (▲), and L-tryptophan at pH* 3.0 (×) are presented. To compute the overall concentration of Cl^- and I^- ions, the concentrations of NaCl and DCl were summed with the ion concentration added. The λ_{max} of I at pH* 4.2 (with 10 mM sodium acetate) and N at pH 5.3 (10 mM sodium acetate) are presented as dashed lines for comparison. The measurements were performed at 20.0 °C.

The effects on the structure of apomyoglobin are anion-dependent, and Cl^- and I^- show some differences in experiments carried out on myoglobin (*25*). It seems clear from Figure 2 that a structural difference, however, cannot explain the very different nature of the emission λ_{max} titration of Cl^- versus I^-. The emission λ_{max} of apoMb for an I^- concentration of greater than ~20 mM is more blue shifted than even that of the native state which is the most compacted state of apoMb; iodide could not cause such a drastic change in compactness at this low pH. To further examine if the structural change caused by Cl^- is essentially similar to that caused by I^-, melting experiments were performed using IR spectroscopy, which is also sensitive to core formation. It was found that E conformations formed with either Cl^- and I^- melted identically (see below; comparative CD studies could not be performed due to iodide absorption). In addition, the relaxation kinetics of E were the same using either Cl^- or I^- as the anion (see ref *19*). However, iodide contains absorption bands in the visible and near UV and is a strong quencher of fluorescence. Thus, the most plausible explanation of most of the differences in fluorescence behavior between NaCl and NaI is that one of the two Trp residues is solvent exposed in the E form. Then, iodide's influence is two-fold. First, it drives the U → E transition, like chloride, causing one of the Trps to become solvent protected. Second, it quenches the fluorescence of the exposed Trp residue. This notion is reinforced by the observation that the emission of apoMb at pH* 3.0 with 20 mM NaCl is 25% broader than that at pH* 3.0 with 20 mM NaI (data not shown). Moreover, the pH* 3.0, 20 mM NaCl emission curve is fit well to a scaled sum of the emission curve for apoMb in a minimal salt solution (both Trps are completely solvent exposed) plus the emission curve of apoMb at pH* 3.0 with 20 mM NaI (an emission maximum of a highly buried Trp residue). Furthermore, it has been demonstrated using modified sperm whale apoMb that the fluorescence maximum of Trp14 lies at 326 nm, suggesting a highly buried indole ring, while that of Trp7 lies at 333 nm, indicative of a more water exposed Trp indole ring (*26*). The crystal structure of the holoprotein indicates that Trp7 is greater than 50% exposed in the native form, and UV resonance Raman measurements suggest that it is completely exposed in the I form (*27*).

Figure 3 shows UV CD melting curves of the various acid-destabilized forms of apoMb as well as under "native" state conditions (pH* 5.3) for comparison using the value of the ellipticity at 222 nm as a marker for helical secondary structure. The thermal denaturation transition for the native state exhibits a T_M of 61 °C; this is good agreement with our previous IR measurements (*17*) of the melting of apoMb-N, under the same conditions, which exhibited a T_M of 58 °C for the melting of native-like helices (i.e., using the characteristic IR amide I′ marker band at 1650 cm^{-1}; see below). This thermal denaturation, however, leaves intact the AGH core (*10*). The E form melting transition is also quite clear; $T_m = 43 \pm 0.5$ °C for the sigmoidal portion of the curve. The shape of the melting curve of E (hence, the temperature at which the melting appears to be half over) differs substantially from that determined from fluorescence or IR measurements (see below). Hence, this measurement was repeated by taking the same sample, splitting it into two portions, and simultaneously performing CD and fluorescence measurements. This rules out the possibility that the differences in the melting curves arise from small differences in chemical conditions. The results were consistent with previous measurements.

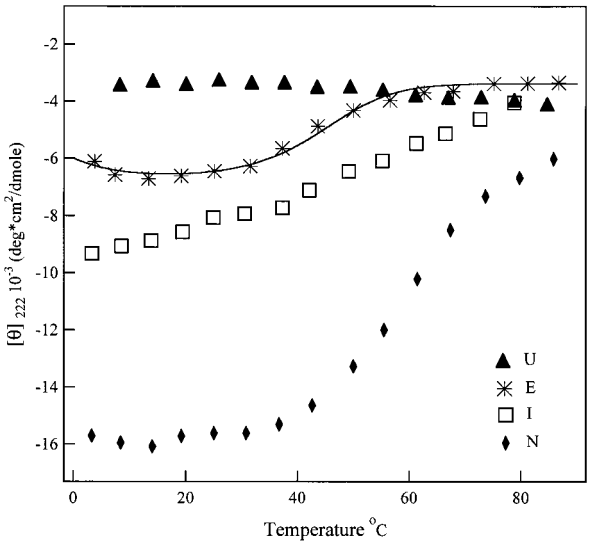

FIGURE 3: Molar ellipticity, [Θ], at 222 nm of apoMb at different pH* values and salt concentrations as a function of temperature. [Θ] values at pH* 2.0 and 2 mM Cl^- [U form (▲)], pH* 3.0 and 20 mM Cl^- [E form (∗)], pH* 3.0 and 250 mM Cl^- [I′ form (□)], and pH* 5.3 and 20 mM Cl^- [N form (♦)] are presented. The solid curve in the van't Hoff analysis fit to the E form data, taking into account a finite heat capacity change between the folded and unfolded structures: $\Delta H = 26 \pm 3$ kcal/mol, $\Delta S = 83 \pm 10$ cal mol^{-1} deg^{-1} at T_m, $\Delta C_p = 950 \pm 100$ cal mol^{-1} deg^{-1}, and $T_m = 43 \pm 0.5$ °C. See ref *29* for the functional form of $\Delta G(T)$.

The UV CD transition for E exhibits long baselines on both sides of the transition so that a reliable van't Hoff analysis could be performed (*28*). This yielded an enthalpy of melting ΔH of 26 ± 3 kcal/mol and an entropy ΔS of 83 ± 10 cal mol^{-1} deg^{-1} at T_m. There is clearly the beginning of cold denaturation in the data of Figure 3 for E; hence, ΔH is temperature-dependent and ΔC_p, which is the difference in heat capacity between the folded and unfolded states, is introduced (cf. ref *29*). The data depicted in Figure 3 do not reach a low enough temperature to determine the cold denaturation midpoint, T_c. However, the approximate midpoint as estimated from the data in ref *10* ($T_c = -8$ °C) yields a ΔC_p of 950 ± 100 cal mol^{-1} deg^{-1}. The curve plotted on top of the E form data in Figure 3 is the fit using the temperature-dependent enthalpy analysis and functional form given in ref *29*. The margin of error is estimated so that the van't Hoff function fits the entire high-temperature melting profile (which essentially fixes ΔH and ΔS at T_m) and has −8 °C as the low-temperature melting point, T_c. Melting of the I′ form does not yield a sigmoidal melting curve; rather, the melting is gradual, covering the entire temperature range. We have previously shown from Trp emission studies that the AGH core is intact for I forms at temperatures up to 60 °C (*10*); the observed melting up to this point presumably has to do with the melting of helices not involved with the core. In fact, the molar ellipticity for the I form at 60 °C is very close to the value for the N form at 80 °C. It should be remembered that the core remains intact during the transition shown in Figure 3 for N (*10*, *17*). A similar thermodynamic analysis for the N form from the data of Figure 3 yielded a ΔH of 28 kcal/mol and a ΔS of 85 cal mol^{-1} deg^{-1} at T_m. However, since the core remains intact during the N form

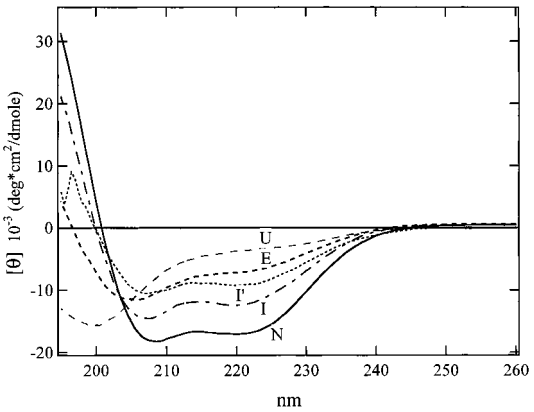

FIGURE 4: CD spectra for the various forms of horse heart apomyoglobin: (—) N (pH* 5.3 and 10 mM NaCl), (— - —) I (pH* 4.2 and 10 mM NaCl), (•••) I′ (pH* 3.0 and 250 mM NaCl), (- - -) E (pH* 3.05 and 20 mM NaCl), and (— —) U (pH* 2.0 and minimal salt).

transition, the melting enthalpies calculated for E and N refer to different structural parts of the protein that are melting.

The CD spectra of I, I′, and N each contain the well-known profile characteristic of an α-helix with minima near 208 and 222 nm (Figure 4). However, the profile of E is slightly different, containing minima at 205 and 222 nm. This is in accord with the IR data (see below), which suggest that E consists of buried polypeptide chains of nonstandard α-helix within the core as opposed to the fully formed standard helices seen in the spectra of I, I′, and N. The CD and IR measurements also show that E and I are substantially different structures. We would estimate from these data that, under the conditions used to produce E here (20 mM NaCl and pH* 3.0), the amount of I (or I′) that is present is less than 25%. Fits to the UV CD data at 20 °C using the program CONTIN (*22*) yielded the following helical fractions: 4% for U, 24% for E, 34% for I′, 50% for I, and 57% for N.

The amide I′ absorption bands of apoMb-E at three different temperatures (above, at, and below the temperature at which the protein is most stable) are presented in Figure 5a. Second-derivative spectra are shown in Figure 5b. Second-derivative spectra under other salt and pH conditions are shown in Figure 6 at 20.3 °C. The FTIR absorbance measurements indicate that E is highly disordered, in agreement with other results (*10*, *11*, *24*). Below the high-temperature melting transition, the multicomponent bands are centered near 1645 cm^{-1}. According to previous assignments (*30*, *31*), two structural types have absorbances close to this frequency in D_2O: α-helices and polypeptide chain without any particular secondary structure that are buried in native proteins. The disordered structure component is very broad because it includes contributions from a wide range of conformations of polypeptide bonds that encounter various hydrogen bonding partners and dipole−dipole couplings (*31*). Usually only one component at 1640−1648 cm^{-1} is assigned to disordered structure of native (folded) proteins (*30*, *31*). However, a second, less intense band at 1668−1675 cm^{-1} is generally observed for unfolded proteins and peptides and assigned to solvent-exposed disordered structure (*21*, *32*, *33*). Second derivatives of the spectra yield peaks at the positions of the component bands, even for the apparently smooth bands of Figure 5a. We assign the two broad bands at 1645 and 1675 cm^{-1} appearing in the second-derivative spectrum

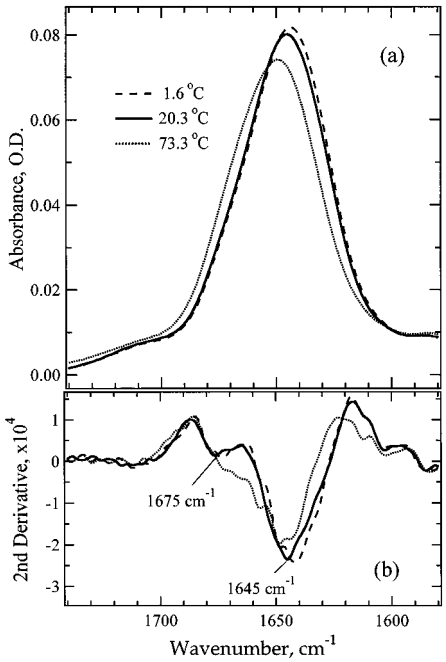

FIGURE 5: Equilibrium FTIR absorbance spectra of apoMb-E (4.4 mg/mL, 20 mM NaCl, pH* 3.0) in the amide I′ spectral region (a) and their second derivatives (b) at 1.6 (- - -), 20.3 (—), and 73.3 °C (•••). The temperature-dependent D_2O background has been subtracted from each FTIR spectrum. The uncertainty in the second-derivative spectrum is given by an examination of the spectra near 1730 cm^1, where there is no protein absorbance; it is about $\pm 1 \times 10^{-5}$.

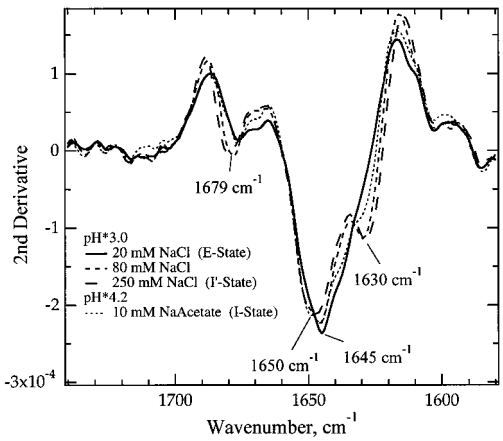

FIGURE 6: Second derivatives of the equilibrium FTIR absorbance spectra of apoMb (4.4 mg/mL) of E, I, and I′ and at intermediate salt concentrations at pH* 3.0 and 20.3 °C. Before the second-derivative calculation, all IR absorbance spectra were reduced to the same maximum absorbance as the E form spectrum shown in Figure 5a. The uncertainty in the second-derivative spectrum is found by an examination of the spectra near 1730 cm^1, where there is no protein absorbance; it is about $\pm 1 \times 10^{-5}$.

of apoMb-E (Figure 5b) to disordered coil in buried and solvent-exposed polypeptide, respectively.

The usual position of the IR amide I′ absorption band of native α-helix is between 1650 and 1655 cm^{-1} (*30*, *31*), close to the position of the main component of disordered structure. However, the native helical component is sharper and thus more pronounced in the second-derivative spectrum. It is observed in the spectra of the more ordered apoMb-N (*16*, *17*) and apoMb-I forms (Figure 6). This component appears only as a weak shoulder in the second derivative of the apoMb-E spectrum. Clearly, the proportion of helices in

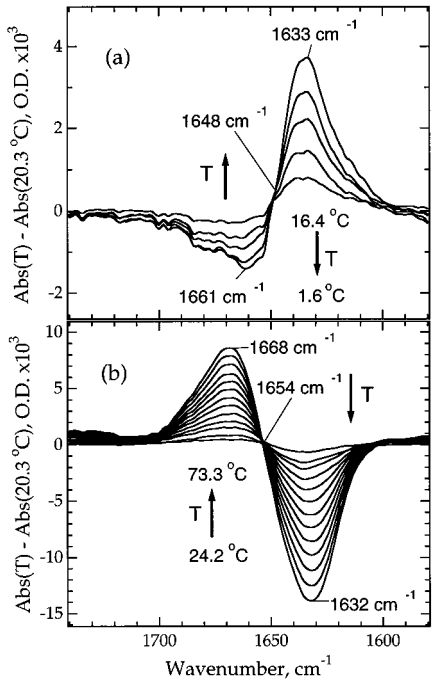

FIGURE 7: Difference FTIR spectra of E form apoMb, generated by subtracting the spectrum at 20.3 °C from the spectra at lower (a) and higher (b) temperatures. See the Figure 5 legend for other details.

native-like surroundings appears to be very small for E, even smaller than in I (*16*). However, the 1650 cm^{-1} band becomes evident at pH* 3.0 with further addition of salt to form I′ (Figure 6). These general observations are in accord with the CD results depicted in Figures 3 and 4 and a recent UV resonance Raman study on horse heart apomyoglobin that found the helical content of the protein decreases with decreasing pH under low-salt conditions (*27*). The amide I′ absorption of α-helices formed by peptides or destabilized proteins is shifted to lower frequencies (1630−1645 cm^{-1}) compared to the frequency of α-helices found in native proteins (*21*, *34*−*37*). This "red" shift is attributed to a greater level of exposure of the helix backbone to water (*17*, *35*, *37*, *38*), hence the label "solvated" helix. A very weak unresolved shoulder is observed at 1630 cm^{-1} in the second-derivative spectrum of E (Figure 6), indicating the presence of some solvated helix. The magnitude of this shoulder decreases with increasing temperature (Figure 5; the temperature-induced change is clear in the difference spectra of Figure 7 which verifies the existence of some IR signal near 1630 cm^{-1} in the spectrum of E) but increases dramatically with further addition of NaCl to form I′ (Figure 6). I, at pH* 4.2, contains fewer solvated helices than the high-salt, low-pH I′ forms, but substantially more than E. It was shown recently that under the conditions which we (and others) used, I is only marginally stable (*14*). The increase in the magnitude of the 1630 cm^{-1} component is coupled with the appearance of a higher-frequency band at 1679 cm^{-1} (Figure 6). One can argue that the observed couple is due to a β-structure which exhibits a characteristic amide I′ doublet. This interpretation is unlikely for two reasons. First, the two amide I′ components of a β-structure are usually found at lower (1617−1628 cm^{-1}) and higher (1675−1687 cm^{-1}) frequencies (*31*, *32*, *39*). Second, an increase in either pH or salt concentration results in a strong increase of helicity according to circular dichroism measurements in the far-UV region (*11*, *24*). The observed increase in the magnitude of the 1679 cm^{-1} band is more likely due to an increased population of turns within the more ordered apoMb forms (*30*, *31*).

E exhibits both high-temperature melting and cold denaturation which can be monitored by fluorescence (*10*) and by CD (Figure 3). The IR absorption spectrum of E also changes with temperature (Figure 5). To elucidate the character of the changes, difference spectra at different temperatures were calculated. The spectrum measured at 20.3 °C (between the denaturation transitions) was subtracted from the others (Figure 7). The major effect is the decrease in the level of absorption around 1633 cm^{-1} with a concomitant absorption level increase at higher frequency with increasing temperature. A similar pattern has been found for helical peptides and other apoMb forms (*16*, *17*, *21*), where it was ascribed to the melting of solvated helices. This major effect is similar in both the cold- and heat-denaturation temperature regimes (panels a and b of Figure 7, respectively). However, there is also a difference in the frequencies of the isosbestic points for the low (1648 cm^{-1})- and high (1654 cm^{-1})-temperature transitions. Given the assignments above, the explanation for this difference is that not only solvated but also native-like helices are melted in the high-temperature transition whereas only native-like helices melt at low temperatures.

The melting behavior of E is further illustrated by plotting the temperature dependence of the Trp fluorescence emission maxima (Figure 8a) and the amide I′ intensities at the structurally sensitive maker band positions (Figure 8b,c). The melting transition of apoMb-E made with 20 mM NaCl (pH* 3.0), as reported by the emission maximum of the indole rings of Trp7 and -14, has been previously determined (*10*). A clear transition is observed. The high-temperature value for the emission λ_{max} is at the same wavelength as that observed for an indole ring free in solution; hence, the AGH core has completely melted. The estimated middle point for the transition is 48 °C. The solid line plotted on top of these data is the van't Hoff analysis fit, using the same functional form that was taken for the similar fit to the E form CD melting data (see above), taking into account the finite heat capacity change between the folded and unfolded structures: $\Delta H = 21 \pm 3$ kcal/mol, $\Delta S = 83 \pm 10$ cal mol^{-1} deg^{-1} at T_m, $\Delta C_p = 750 \pm 100$ cal mol^{-1} deg^{-1}, and $T_m = 48 \pm 0.5$ °C. For apoMb-E in 20 mM NaI (pH* 3.0), a similar transition is observed with, however, significant differences (Figure 8a). The middle point of the transition at 58 °C is much higher than that found for NaCl, and there is slow melting observed from 10 to 55 °C. As outlined above, the substantial differences between the shapes of the two melting curves arise from iodide quenching of the fluorescence quenching, which implies that only the most buried Trp residues are observed in the iodide solutions.

Melting curves using the intensity of the IR absorbance at 1648 cm^{-1}, a frequency close to the maximum position of the absorbance of native helical secondary structure in proteins, were determined for E and for both chloride and iodide salts. The results of this experiment are shown in Figure 8b. In this case, the melting curve shape is not dependent on the anion, suggesting that the E form structure is the same, or at least quite close, for either anion. Moreover,

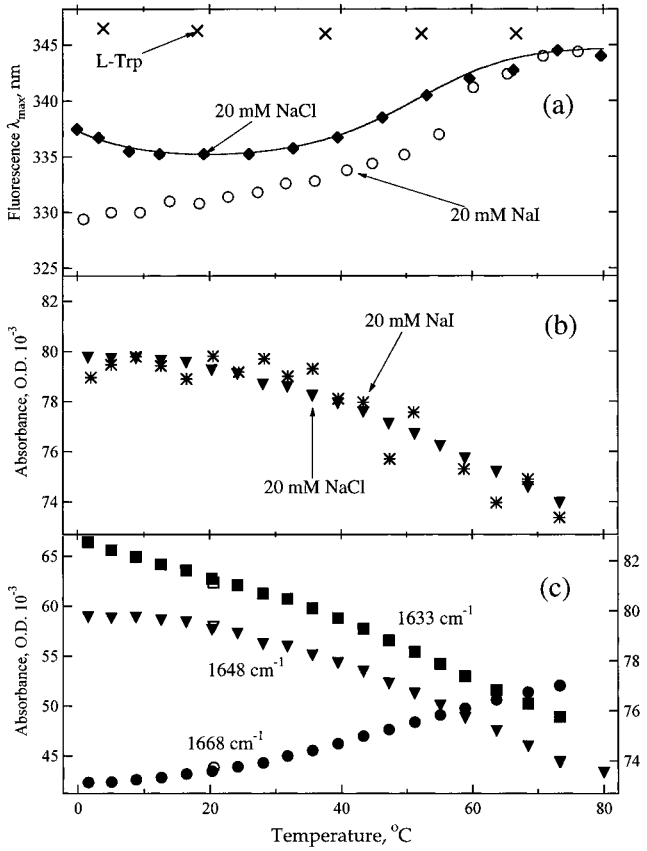

FIGURE 8: Temperature dependencies of spectral parameters of apoMb at pH* 3.0. (a) Fluorescence emission maximum position λ_{max} for 20 mM NaCl (◆) and 20 mM NaI (○) and λ_{max} of L-tryptophan in D_2O (×). (b) IR melting transitions at 1648 cm^{-1} for 20 mM NaCl (▼) and 20 mM NaI (∗). The OD of the sample containing NaI has beed reduced by 0.0175. (c) IR melting transitions measured at key wavenumbers: 1633 (■), 1648 (▼), and 1668 cm^{-1} (●) (the white symbols are the values found after returning the sample from the highest temperature). The left scale is for 1633 and 1668 cm^{-1}; the right scale is for 1648 cm^{-1}. See the Figure 3 legend for other details. The solid curve is the van't Hoff analysis fit to the E form data (panel a), taking into account a finite heat capacity change between the folded and unfolded structures: $\Delta H = 21 \pm 3$ kcal/mol, $\Delta S = 83 \pm 10$ cal mol^{-1} deg^{-1} at T_m, $\Delta C_p = 750 \pm 100$ cal mol^{-1} deg^{-1}, and $T_m = 48 \pm 0.5$ °C. See ref *29* for the functional form of $\Delta G(T)$.

the shape shows a temperature dependence substantially different than that found in the CD or fluorescence study. The curve exhibits a slope bend at ~30 °C, which coincides approximately with the major melting transition according to CD (Figure 3) and somewhat preceding the transition found in the fluorescence measurements (Figure 8a). Thus, this helical type almost certainly exists within the tight AGH core stabilized by the same cooperative interactions that then show up in sigmoidal melting behavior of the Trp emission maxima (*10*). A determination of a reliable value for the T_M of the sigmoidal-like melting shown at 1648 cm^{-1} between 30 and 80 °C is difficult since the transition is very wide and may not yet have leveled out at the highest temperature that has been measured.

The amide I component at 1633 cm^{-1} yields a melting transition that is essentially linear with a steep slope (Figure 8c). The absorbance at this frequency is dominated by solvated helices; hence, the extent of their melting is approximately the same throughout the whole temperature range that was measured. This pattern is the same as the melting behavior found previously for the solvated helical component of other apoMb forms as well as of model helical peptides (*16, 17, 21*). Some slope bend at 30 °C is also observed for the 1633 cm^{-1} temperature dependence. This may be due, at least partially, to the overlapping of the native helix absorbance band with the solvent-exposed helix marker band. More likely, however, core melting probably influences the fraction of solvated helices.

The transition measured at 1668 cm^{-1} has complex character. As the melting of both helical types, solvated and buried native-like, results in a disordered solvent-exposed polypeptide which is typically observed near 1668 cm^{-1}, both the steep slope of the solvated helices melting and the 30 °C bend should be found in the 1668 cm^{-1} temperature dependence. This, in fact, is observed at and above room temperature. However, the decrease in the fraction of solvated helices between 0 and 15 °C does not coincide with the increase in the disordered chain fraction. Hence, native helices increase their fraction proportionately at the expense of the solvated helices moiety with renaturation from the cold-denatured state. This phenomenon is consistent with a hydrophobically driven process of packing helices together and removing water. The different patterns of the high-frequency absorption bands found in the difference spectra for the cold- and heat-denaturation regions (Figure 6) also support this conclusion since (1) the low-temperature difference spectra exhibit a wider high-frequency bandwidth which may well comprise a native helix component in addition to the disordered component and (2) the isosbestic point in the cold denaturation has shifted toward the marker position for solvated helix compared with the heat-denatured position.

DISCUSSION

We have studied the structures of various acid-destabilized forms of apoMb and the thermodynamic melting behavior of E using three probes of structure: the fluorescence emission of apoMb's two tryptophan residues, UV CD, and IR absorption in the protein's amide I′ absorption band. The degree of solvent screening of the indole ring of Trp residues is obtained from measurement of their emission maxima. The two Trp residues of horse apoMb are fortuitously located at positions 7 and 14 of the A helix, where A comes into contact with the G and H helices during core formation. Consequently, the indole rings become solvent protected upon formation of the AGH core. The sensitivity of indole fluorescence emission maxima to the hydrophobicity of their surroundings and the presence of the only two Trps of apomyoglobin in a helix central to core formation make fluorescence emission a very sensitive indicator of the formation of the AGH core. The IR absorption in the amide I′ region is a complementary structural probe because it contains marker bands for helices which are buried within the hydrophobic environment of proteins (at 1650−1655 cm^{-1}), helices which are solvated (1630−1655 cm^{-1}), and both buried and solvated disordered structures (approximately 1645 and 1665 cm^{-1}, respectively). The value of the far-UV CD at 222 nm has been widely employed as an indicator of the amount of helical structure in native and partially folded proteins, although the length dependence of the induced helical CD signal may hinder detection of short runs of solvated helix. The fluorescence measurements probe a

specific structure change, the solvent accessibility of the indole rings, which is determined primarily by the immediate environment, although this in turn is influenced by the global conformation. The complementary CD and IR techniques report on global secondary structure content, but IR absorption is also influenced by the formation of specific tertiary structures, such as helix−helix packing which excludes solvent.

Comparison of the I Form Structures. Both I forms are generally similar to one another in structure and melting behavior. Both contain buried helices as well as solvated helices as indicated by the marker bands in their IR amide I′ spectra; both contain buried Trp indole rings as found in the native form of the protein, and both contain a stable core which does not melt except at very high temperatures (*10*). These results are in general agreement with multidimensional NMR (*4*) studies of sperm whale apoMb-I which also indicate a compact core and dynamical fluctuating regions outside the core, most notably in the C and D−E regions and the C-terminus that sample helical backbone conformations.

The AGH core is disrupted only under the most destabilizing chemical conditions (pH 2 and minimal anion concentrations). The melting experiments show that no other tertiary contacts are present (which we define as a number of interacting residues melting together to yield a cooperative-like melting transition) except under conditions where the AGH core is formed (i.e., pH >2 and/or high salt). On the other hand, some secondary structure exists even for the unfolded "U" state since there are residual far-UV CD signals (Figures 3 and 4). Indications from UV resonance Raman studies (*27*) and multidimensional NMR (*4*) studies of apoMb and NMR studies of peptide fragments of apoMb (*40*) show that U contains helical structure in the H helix region and has significant helical propensity for A and between residues 52 and 61 (part of E, the D−E link, and the first loop in E in the native protein). The stability of the AGH core relative to the rest of the protein and the strong helix propensity of its components suggest that the peptide sequence of apoMb is coded in such a way that (1) tertiary contacts are not made easily apart from the core and (2) the specific sequence of the A and G−H peptide runs are such as to facilitate the formation of tertiary contacts within the core.

Structure of E. The highly destabilizing chemical conditions resulting in E form apoMb yield a quantitatively different structure as compared to the I forms. E contains a corelike structure formed by the association of a portion of the would-be A helix with the central portion of the G−H peptide. Although this core has a sufficient number of tertiary contacts to yield a high-temperature sigmoidal melting curve (indicative of a cooperative transition), the size of this core is smaller than in I or the native form of the protein as shown by the CD results. The IR results suggest that within the AGH core, E contains a significant proportion of buried disordered runs of polypeptide structure in contrast to the α-helical structure found in the AGH core of apoMb-N or -I. Moreover, it appears that the indole ring of Trp7 is mostly if not completely solvent exposed in E while Trp14 is buried to varying degrees. Hence, the final tertiary contacts found in the AGH core of apoMb-N have not yet fully formed in E. This is probably the reason that the sigmoidal melting transition of E has a T_M value for core melting below those of any of the I forms; there are on average a fewer tertiary contacts. In addition, E consists of multiple conformers which would yield a higher value of entropy compared to I; this too would depress T_M. E also has an amount of solvated helices that is smaller than that in I. The CD measurements suggest that 24% of the protein is in a "helical-like" environment, or ∼36 residues. The size of the core is no more than this since E likely contains similar helical sections as found by NMR for U, some of which are outside the core volume (*4*).

One of the most significant structural attributes of E is that it is highly heterogeneous, consisting of multiple conformations each of which retains some portion of the AGH core. Several lines of evidence support this view. While it is clear that E undergoes a sigmoidal high-temperature melt in all cases, the nature of the melting transition that is observed (CD, Trp emission, and IR) varies depending on the spectroscopic technique employed and hence the specific structural attribute which is probed. Second, the IR amide I′ absorption of E shows a maximum at a position indicative of disordered but buried amides compared to the maximum position in the spectra of I which indicates buried α-helices (a more ordered structure). Third, our results and previous studies (*27*) suggest that the indole ring of Trp7 is solvent exposed. However, the indole ring of Trp14 is buried but apparently to different degrees depending on the conformational state of E. This is surmised because the emission maxima from samples in NaCl are broader than that found in NaI and never reach, even at the highest NaCl salt concentrations, the more blue shifted emission maximum from protein in NaI solutions at concentrations of ≥15 mM (see the Results). Only the conformations containing the most highly protected Trp14 are visible in the NaI experiments due to quenching by the iodide anion, whereas partially protected conformations are detected in NaCl, shifting the apparent λ_{max} to a higher wavelength. Last, ref *19* reports kinetics results from temperature-jump studies on E form apoMb that show different relaxation times (10−70 μs) depending on the spectroscopic probe used to monitor the changes in structure.

A structural explanation for this heterogeneity, particularly concerning the structures that give rise to the varying emission spectra of the indole ring of Trp14 observed in apoMb-E, is suggested by what is known about the structure of the I form. Figure 1 shows the completely folded protein, and it can be seen that the indole ring of Trp14 is sandwiched between the H and E helices. However, the E helix is not formed in apoMb-I (*4*) and therefore is likely to be absent in the more destabilized apoMb-E. This would presumably allow the indole ring of Trp14 to adopt non-native associations within the AGH core structure. Some of these associations could include a largely buried ring which would explain the strongly blue shifted emission spectra found in the iodide solutions, and some could include a completely exposed indole ring whose emission spectra would change little when the unfolded protein forms apoMb-E.

Thermodynamics of Heat and Cold Denaturation of E. The lowest temperatures reached in our study are close to 5 °C, but the cold-denatured transition is lower than this, about −8 °C (*10*). Hence, our results only report on the very earliest portion of cold denaturation. However, it is clear that for both the cold and heat unfolding transitions, the E conforma-

tions, whose Trp14 indole ring is buried, becomes exposed since the emission maxima shift from a low wavelength toward the value of a solvent-exposed indole ring. However, the results suggest that the natures of the cold- and heat-denatured transitions are different. At low temperatures, the acid-destabilized protein gains runs of solvated helices as the temperature is lowered, even as the Trp14 indole ring becomes solvent exposed. This is consistent with the dissociation of the A helix from the core, as previously postulated for cold denaturation of N form apoMb (*41*). In the high-temperature melting, not only does buried desolvated disordered and helical polypeptide chain melt more or less concomitantly with solvent exposure of Trp14, but solvated helices that may or may not be associated with the core also melt.

The change in heat capacity as E unfolds is quite large. The actual value obtained from the van't Hoff analyses depends on the spectroscopic probe used to measure the transition: $\Delta C_p = 950 \pm 100$ cal mol^{-1} deg^{-1} melting monitored by CD compared to $\Delta C_p = 750 \pm 100$ cal mol^{-1} deg^{-1} from Trp emission (see the Results). Since Trp emission likely more accurately monitors just core formation, the ΔC_p from Trp emission is likely more accurate. In any case, either value suggests that a large number of hydrophobic residues are exposed to solvent in the transition as this is the main effect in determining the size of ΔC_p (*42*). Using a rough average value of ΔC_p of unfolding of ~22 cal deg^{-1} mol^{-1} per residue as is appropriate for apomyoglobin (*43*), approximately 34−43 residues take part in the melting, which is comparable to the number of residues which form the core in E given by the CD results (see above). Clearly, the melting must involve solvating substantial hydrophobic surface area. The change in the enthalpy upon melting is also quite large. ΔH at the heat-denaturation point of 26 ± 3 kcal/mol averaged over 36 residues is 0.7 kcal/mol per residue.

Implications for the Folding of ApoMb. If it is assumed that the acid-destabilized forms of apomyoglobin resemble the earliest formed structures on the folding pathway of the protein, the heterogeneity of the E form yields interesting insight into the energy landscape of the folding process. The picture that emerges is one of a compact intermediate without a precisely fixed structure, but rather having considerable conformational flexibility. The heterogeneous nature of E is consistent with the folding funnel view, in which the number of conformations sampled increases as the system is destabilized. In this picture, enthalpy is traded for entropy along the folding pathway. Importantly, it is emphasized that there are many different pathways to the more folded structures and there are multiple structures for these. As a representative of the first forms of folded structure, E however contains more specific sets of tertiary interactions (only A with G and H) than is generally imagined in the funnel picture or in pictures which emphasize general hydrophobic collapse with few fixed tertiary contacts. The formation enthalpy of E is comparatively large, and the amount of entropy shed is likewise large.

The transition from E to I involves a further collapse of the protein, with changes in both secondary and tertiary structure, although these changes are more subtle then in the U to E collapse. The buried disordered runs of polypeptide in the core of E convert to α-helix, and this likely involves a reduction in the number of conformational states or conformational heterogeneity as well. In addition, the amount of solvated helices grows in I. I is considerably more helical than E. Studies of sperm whale apomyoglobin under conditions resembling the E to I transition, called the I_a to I_b transition (*9*), suggest that the two species are separated by a kinetic barrier. The further collapse of I to form the native form of apoMb involves the formation of more secondary structure and another set of apparently fixed tertiary contacts involving the B and E helices (*3*, *17*). This event represents a second "condensation" event as the number of fixed tertiary contacts that are formed is quite large.

REFERENCES

1. Eliezer, D., and Wright, P. E. (1996) *J. Mol. Biol. 263*, 531−538.
2. Lecomte, J. T. J., Kao, Y. H., and Cocco, M. J. (1996) *Proteins 25*, 267−285.
3. Jennings, P. A., and Wright, P. E. (1993) *Science 262*, 892−896.
4. Eliezer, D., Yao, J., Dyson, H. J., and Wright, P. E. (1998) *Nat. Struct. Biol. 5*, 148−155.
5. Tsui, V., Garcia, C., Cavagnero, S., Siuzdak, G., Dyson, H. J., and Wright, P. E. (1999) *Protein Sci. 8*, 45−49.
6. Griko, Y. V., Privalov, P. L., Venyaminov, S. Y., and Kutyshenko, V. P. (1988) *J. Mol. Biol. 202*, 127−138.
7. Hughson, F. M., Wright, P. E., and Baldwin, R. L. (1990) *Science 249*, 1544−1548.
8. Barrick, D., and Baldwin, R. L. (1993) *Protein Sci. 2*, 869−876.
9. Jamin, M., and Baldwin, R. (1998) *J. Mol. Biol. 276*, 491−504.
10. Gilmanshin, R., Dyer, R. B., and Callender, R. H. (1997) *Protein Sci. 6*, 2134−2142.
11. Nishii, I., Kataoka, M., and Goto, Y. (1995) *J. Mol. Biol. 250*, 223−238.
12. Kay, M. S., and Baldwin, R. L. (1996) *Nat. Struct. Biol. 3*, 439−445.
13. Lecomte, J. T. J., Kao, Y. H., and Cocco, M. J. (1996) *Proteins: Struct., Funct., Genet. 25*, 267−285.
14. Luo, Y., Kay, M. S., and Baldwin, R. L. (1997) *Nat. Struct. Biol. 4*, 925−930.
15. Gilmanshin, R., Callender, R. H., and Dyer, R. B. (1998) *Nat. Struct. Biol. 5*, 363−365.
16. Gilmanshin, R., Williams, S., Callender, R. H., Dyer, R. B., and Woodruff, W. H. (1997) *Biochemistry 36*, 15006−15012.
17. Gilmanshin, R., Williams, S., Callender, R. H., Woodruff, W., and Dyer, R. B. (1997) *Proc. Natl. Acad. Sci. U.S.A. 94*, 3709−3713.
18. Dyer, R. B., Gai, F., Woodruff, W., Gilmanshin, R., and Callender, R. H. (1998) *Acc. Chem. Res. 31*, 709−716.
19. Gulotta, M., Gilmanshin, R., Callender, R. H., and Dyer, R. B. (2001) *Biochemistry 40*, 5137−5143.
20. Crumpton, M. J., and Polson, A. (1965) *J. Mol. Biol. 11*, 722−729.
21. Williams, S., Causgrove, T. P., Gilmanshin, R., Fang, K. S., Woodruff, W. H., Callender, R. H., and Dyer, R. B. (1996) *Biochemistry 35*, 691−697.
22. Provencher, S. W., and Glockner, J. (1981) *Biochemistry 20*, 33−37.
23. Geierstanger, B., Jamin, M., Volkman, B. F., and Baldwin, R. L. (1998) *Biochemistry 37*, 4252−4265.
24. Fink, A. L., Calciano, L. J., Goto, Y., and Palleros, D. (1991) in *Conformations and Forces in Protein Folding* (Nall, B. T., and Dill, K. A., Eds.) pp 169−174, American Association for the Advancement of Science, Washington, DC.
25. Goto, Y., Takahashi, N., and Fink, A. L. (1990) *Biochemistry 29*, 3480−3488.

26. Postnikova, G. B., Komarov, Y. E., and Yumakova, E. M. (1991) *Eur. J. Biochem. 198*, 223.
27. Chi, Z., and Asher, S. (1999) *Biochemistry 38*, 8196−8203.
28. Griko, Y. V., and Privalov, P. L. (1994) *J. Mol. Biol. 235*, 1318−1325.
29. Fersht, A. (1999) *Structure and Mechanism in Protein Science: A Guide to Enzyme Catalysis and Protein Folding*, Freeman and Co., New York.
30. Susi, H., and Byler, D. M. (1986) *Methods Enzymol. 130*, 290−311.
31. Surewicz, W. K., and Mantsch, H. H. (1988) *Biochim. Biophys. Acta 952*, 115−130.
32. Chirgadze, Y. N., Shestopalov, B. V., and Venyaminov, S. Y. (1973) *Biopolymers 12*, 1337−1351.
33. Gilmanshin, R., Van Beek, J., and Callender, R. (1996) *J. Phys. Chem. 100*, 16754−16760.
34. Chirgadze, Y. N., and Brazhnikov, E. V. (1974) *Biopolymers 13*, 1701−1712.
35. Haris, P. I., and Chapman, D. (1995) *Biopolymers 37*, 251−263.
36. Martinez, G., and Millhauser, G. (1995) *J. Struct. Biol. 114*, 23−27.
37. Reisdorf, W. C., Jr., and Krimm, S. (1996) *Biochemistry 35*, 1383−1386.
38. Manas, E. S., Getahun, Z., Wright, W. W., DeGrado, W. F., and Vanderkooi, J. M. (2000) *J. Am. Chem. Soc. 122*, 9883−9890.
39. Prestrelski, S. J., Byler, D. M., and Thompson, M. P. (1991) *Int. J. Pept. Protein Res. 37*, 508−512.
40. Waltho, J. P., Feher, V. A., Merutka, G., Dyson, H. J., and Wright, P. E. (1993) *Biochemistry 32*, 6337−6347.
41. Sabelko, J., Ervin, J., and Gruebele, M. (1998) *J. Phys. Chem. B 102*, 1806−1819.
42. Makhatadze, G. I., and Privalov, P. L. (1990) *J. Mol. Biol. 213*, 375−384.
43. Privalov, P. L., and Makhatadze, G. I. (1990) *J. Mol. Biol. 213*, 385−391.

BI002255V